1   Science Plan

1.1   Scientific Justification

1.1.1   Old Stars in Extended Ultraviolet Disks

The size of a galaxy is a fundamental parameter in our understanding of the evolution of galaxies. In λCDM models, galactic disks are built through mergers and the accretion of small satellites, as well as through *in situ* star formation activity (e.g., Abadi et al. 2003; Governato et al. 2004). These two growth mechanisms have distinctly different predictions for the age of the associated extended stellar population.

According to the inside-out galaxy formation scenario, the outer disk should be dominated by a smoothly distributed young population of stars (Avila-Reese & Firmani 2000). In this model, outer disk stars were either formed from star formation occurring in the galaxy outskirts, or they were transported from the inner disk regions through 'radial migration' (Roškar et al. 2008). GALEX observations have shown the young stellar distribution to extend well beyond the de Vaucouleurs radius R_{25} in the so-called extended UV disk or 'XUV' galaxies (Thilker et al. 2007; Gil de Paz et al. 2007a; Zaritsky & Christlein 2007). In a study of 458 galaxies Wang et al. (2011) find that galaxies fitting the inside-out picture of disk formation are rich in HI and have bluer, more actively star-forming outer disks, consistent with recent simulations (Bush et al. 2010). In a multi-wavelength study of 161 spirals, Muñoz-Mateos et al. (2007) detect a mild positive rise with radius in the specific star formation rate, tentative support for gradual inside-out disk build-up in the majority of systems. However, for a small subset of disks they observe significantly longer disk scalelengths in the UV compared to the NIR, suggesting a period of substantial recent disk growth.

In contrast to inside-out disk formation scenarios, accretion models predict that the diffuse, outermost stellar distribution is largely composed of the remnants of previously accreted satellites and tidal debris from major mergers, and thus is dominated by an older stellar population that likely exhibits substructure (Robertson et al. 2004). The Keck-based work of Ibata et al. (2005) presents such a scenario for M 31: they find stars associated with that galaxy as far as 70 kpc ($1.6R_{25}$) from the nucleus, and with velocities close to those expected for circular orbits at that distance. This stellar emission shows substructure, consistent with an accretion history. Likewise, HST provides evidence for hierarchical assembly of M 31 through a 10 Gyr stellar population 35 kpc from its nucleus (Brown et al. 2008).

Similarly, Thilker et al. (2005) find knots of UV emission extending out to $4R_{25}$ in M 83, a galaxy known to have substructure in its outer disk, perhaps due to an encounter with NGC 5253 1–2 Gyr ago. Dong et al. (2008) and Alberts et al. (2011) use GALEX and IRAC to determine the ages and stellar masses of stars in the XUV disks of six nearby galaxies, finding typical ages of 100–200 Myr, but extending up to over a Gyr. Likewise, Gogarten et al. (2009) find long durations for the star formation history of the outer disk of M 81. Finally, in another study of extended stellar emission in local galaxies, Herbert-Fort et al. (2009) probe the blue and red stellar populations in NGC 3184 out to and beyond $1.6R_{25}$. Though NGC 3184 lacks any obvious young outer disk component, in this galaxy red stellar clusters are more prominent than their blue counterparts at the largest radii, and in fact, the red knots appear to be correlated with the outermost HI at $1.7R_{25}$.

The XUV disk fraction has been estimated to be $\sim$30% (Thilker et al. 2007; see also Zaritsky & Christlein 2007). Thilker et al. separate the XUV galaxies into two classes. Type 1 disks contain filamentary, outer disk substructure, perhaps indicative of an accretion

history or interaction-driven evolution, whereas Type 2 XUV galaxies exhibit a UV profile smoothly extending from the interior to the outer disk regions. Pohlen & Trujillo (2006) find that only 10% of their 90 galaxies show a smooth exponential decline to the edge of their disks; the remaining 90% show double exponential profiles. Two-thirds of the latter subset show steeper declines in the outer regions ('downbending') while one-third exhibit shallower outer profiles ('upbending'). In other words, 30% of galaxies show an increasing surface brightness of optical stellar emission in the outer disks, and 30% show XUV emission.

1.1.2 Hα in Galaxy Peripheries and Other Low Surface Brightness Regions

Star formation has long been thought to occur only above a certain threshold in gas density (Kennicutt 1998; Leroy et al. 2008; Krumholz et al. 2009). Like most other tracers of the interstellar medium, the neutral and molecular gas surface brightness profiles decrease at large galacto-centric radii (e.g., Regan et al. 2006), and thus it is not surprising that Hα surface brightness profiles typically show a sharp truncation near the R_{25} optical edge of galaxies (e.g., Martin & Kennicutt 2001; Elmegreen & Hunter 2006). However, spurred in part by the discovery of XUV disks, sensitive Hα observations in the outer disks of galaxies have shown a more complicated situation, with some Hα profiles extending to 1.5–2R_{25} (Christlein et al. 2010; Goddard et al. 2010). The existence of pockets of star formation in the outer disks of galaxies has important implications for how galaxies grow in areas of low metallicity and gas surface density, and elevated shear and H_{I}/H_2 ratios (Bigiel et al. 2010).

An intriguing result stems from an Hα+UV study of a large sample of nearby galaxies. At star formation rates down to $\sim 10^{-4}$ $M_\odot$ yr^{-1}, comparable to environments in the galaxy outer disks, Lee et al. (2009) find that Hα systematically underestimates the star formation rate relative to the FUV (see also Meurer et al. 2009). One compelling plausible scenario is a steeper IMF resulting in a deficit of high-mass stars, a scenario supported by theoretical predictions (Kroupa & Weidner 2003; Weidner & Kroupa 2006; Pflamm-Altenburg et al. 2009). However, some comparisons of UV and Hα outer disk data point to stochasticity in high-mass star formation as the culprit and provide no evidence for an IMF that is unique to such peripheral environments (Goddard et al. 2010; Alberts et al. 2011). Similarly, Fumagalli et al. (2011) find that stochastic sampling of a standard IMF can reproduce the observed Hα/FUV ratios over a wide dynamic range of star formation rates. In addition, Weisz et al. (2012) successfully modeled the decline in Hα/FUV via bursty dwarf star formation histories.

1.1.3 Science Questions and Goals

All of these results demonstrate a complex variety of morphologies at different wavelengths in the outer disk environment. Does the Type 1 to Type 2 ratio in XUV disks reflect the ratio of accretion-to-inside-out formation scenarios? As the inside-out disk formation theory might suggest, are Type 2 XUV galaxies also 'XHα' galaxies showing a smooth distribution of recent star formation in the outer disk regions? Likewise, according to the scenario whereby galaxies grow by accreting older stars from satellites and tidal debris, are Type 1 XUV galaxies also 'XIR' galaxies showing extended NIR emission that is perhaps clumpy? To be more specific, stellar ages can help to address the question of disk formation, and the Hα equivalent widths along with the IR−UV and FUV−NUV colors can be utilized to determine the ages of the outer disk stellar populations. Combined with the morphology of the stellar emission in the outer disks, such information can help to confirm or reject formation by accretion or formation via an inside-out process.

Another interesting issue is related to what is seen for the galaxies with the smallest star formation rates. Perhaps highly inefficient star-forming outer regions produce only faint stellar outer disks, characterized by a break relative to the inner disks. Likewise, is there a characteristic mass surface density and/or profile inflection for XUV disks, which could provide a unique method for detecting UV-dormant extended galaxies? How do the radial profiles compare at the three different wavelengths—are there any discernible trends in the break radius as a function of stellar population age?

We propose to obtain very deep 3.6 and 4.5 μm imaging of a sample of nearby galaxies, with two primary goals: constraining the age range of UV-bright knots of star formation in the outer disks, and quantifying how far out the evolved stellar population can be detected, yielding its mass surface density and crucial insights into the fossil record in galaxy peripheries. The combination of GALEX and IRAC data will provide a unique leverage for determining ages almost independently of IMF variations (Alberts et al. 2011), while the Hα will trace the ionizing photons of the most massive (and youngest) stars. Dust attenuation will be minimized in the outer disk regions where the dust surface density is low.

1.1.4   Why *Spitzer*?

The apparent size of a galaxy depends on the emission mechanism in question along with the sensitivity of the measurement. Comparing the full extent of the stellar disk traced by old stars to that traced by young stars is technically challenging, particularly for ground-based NIR observations due to variable sky levels. To optically measure the older stellar population requires significantly longer integration times than with *Spitzer* to achieve similar sensitivity to stellar mass; for instance, R band imaging on a 4-m class telescope requires $\sim$50 times the integration time to achieve a similar depth as our *Spitzer* 3.6 μm imaging. Figure 2 displays the UV, optical, and NIR surface brightness profiles and the stellar mass surface density profiles for the XUV galaxy NGC 5474, along with a Cycle 6 example that meets our desired sensitivity. Even if outer stellar disks could be securely detected in the optical, conversion from observed optical surface brightness to stellar mass density is highly dependent on the assumed stellar population age, initial mass function, and metallicity. Thus, observations with *Spitzer* is the only possible approach that will allow us to trace the stellar distribution to unprecedented levels at wavelengths that are insensitive to dust extinction and the galaxy's star formation.

1.2   Technical Plan

1.2.1   Sample Definition

Our sample of XUV galaxies originates from the comprehensive GALEX UV Atlas of Nearby Galaxies (Gil de Paz et al. 2007). Galaxies with UV emission significantly beyond the R_{25} radius were identified via UV surface brightness profiles. Gil de Paz and collaborators have undertaken a comprehensive ground-based campaign at Calar Alto to follow-up these XUV targets with deep broadband and Hα imaging. Focusing on XUV galaxies with deep ancillary data allows for a detailed comparison of the spatially extended stellar populations spanning a wide range of ages. We have taken this subsample of the GALEX Atlas and further selected only moderate-size $(D_{25} < 5.5')$, high Galactic latitude galaxies $(|b| > 35°)$ within 20 Mpc that lack nearby companions, leaving us with a total of 12 XUV galaxies. Excluding galaxies at low Galactic latitudes minimizes contamination by foreground stars, and selecting only

those with major optical diameters smaller than 5.5′ avoids excessively long AORs. Adding a distance cut ensures reasonable spatial resolution—a 7″ surface brightness profile bin width, for example, corresponds to 0.3 kpc at 10 Mpc. The balance between Types 1 and 2 XUV disks is similar to that found in the larger galaxy population found by Thilker et al. (2007).

To enable a fair interpretation of the XUV galaxies, we will use as a control sample the non-XUV galaxies in the EDGES Exploration Science program (PID 80025). This program is obtaining equally-deep IRAC observations for 92 nearby galaxies (cz <1100 km s^{-1}) that span a range in inclination angle, luminosity, and environment. Moderate depth GALEX observations are available for over half of the sample, and deep ground-based optical imaging has been obtained for over 90%. The control sample includes a similar range of morphologies and optical sizes as those found in the XUV sample; issues such as foreground/background contamination and flat-fielding will be similar for the primary and control samples.

As this project requires deep imaging with well-defined sky levels, we used SPOT to determine the typical infrared sky level for each target at both 3.6 and 4.5 μm. In all cases, the expected infrared sky levels are low, less than 100 kJy sr^{-1}. Taken as a whole, our survey of very deep 3.6 μm imaging will allow us to compare the extent and nature of the diffuse stellar distributions in galaxies exhibiting a wide variety of physical characteristics.

1.2.2   Observing Plan

We have analyzed the UV surface brightness profiles of our 12 XUV galaxies. The average R_{UV}/R_{25} ratio for our XUV targets is 2.9. In terms of the 3.6 μm extent, analysis of our deep Cycle 6 data on H I extended galaxies shows some 3.6 μm surface brightness profiles extend beyond $3 - 4R_{25}$. Our proposed 3.6 μm observations are thus designed to map at least to $5R_{25}$. This will ensure enough coverage to adequately sample any extended stellar distributions while still allowing ample area for determining the sky value.

AORs are constructed using the successful strategy utilized for our Cycles 6 and 8 programs. Mosaics are built upon a grid of 100″ spacings ($\sim$one-third the IRAC field of view). Two sets of maps will be obtained for each source to enable asteroid removal and data redundancy, and to build up the map sensitivity to the desired level. Thus, at any given location within the map cores there will be a total of 18×100 s frames resulting in a net integration per sky position of 1800 s (along with a 1200 s $\sim$100″-wide "inner periphery" and a 600 s $\sim$100″-wide "outer periphery"). The smallest maps will be 8x8 mosaics, ensuring at least 10′ map cores at the deepest 1800 s effective integration. We will center the mosaics for 3.6 μm observations, but even our smallest maps have sufficient sky coverage that the field of view of the corresponding 4.5 μm mosaic will include the galaxy as well.

Our sample is restricted to galaxies with low infrared sky levels (less than 100 kJy sr^{-1} at 3.6 μm), and thus we expect to achieve a 1σ noise level per pixel of 0.0018 MJy sr^{-1} at 3.6 μm (based on our Cycles 6 and 8 data and on SENS-PET predictions). Further, the simultaneous images at 4.5 μm will have a per pixel surface brightness sensitivity of 0.0027 MJy sr^{-1}; while the 4.5 μm mosaic will not be centered on the galaxy, it will provide both an independent observation of the extended stellar distribution and provide the potential to trace the faint stellar population to even larger radii (along the axis of observation).

These deep mosaics will trace the stellar distribution to unprecedented levels of a few 0.01 $M_\odot$ pc^{-2}, at wavelengths relatively insensitive to dust and star formation history. Indeed, the 1800 s integration per position would be much deeper than other surveys of nearby galaxies, e.g., SINGS ($N_{\mathrm{gal}} = 75; T$=240 s; Kennicutt et al. 2003), LVL ($N_{\mathrm{gal}} = 258; T$=240 s;

Dale et al. 2009), S^{4}G ($N_\mathrm{gal} \sim 2300$; T=240 s; Sheth et al. 2010), and the IRAC GTO project ($N_\mathrm{gal} = 100$; T=60 or 150 s; Pahre et al. 2004). These surveys reach a 1σ sensitivity of a few to several kJy sr^{-1}, which is typically at the 5% level with respect to the near-IR sky surface brightness (Regan et al. 2006). With ($7''$) azimuthal averaging, our observations will go to 0.2 kJy sr^{-1}, necessary for achieving high S/N in faint outer disks. For comparison, WISE achieves a 3.4 μm sensitivity larger than 1 kJy sr^{-1} over a $5' \times 5'$ area (Wright et al. 2010).

1.2.3 Data Processing

The post-pipeline processing of the data should be straightforward, given our substantial experience with SINGS, LVL, and Cycles 6 and 8 programs. The multi-epoch, multiple-pointing observations for each galaxy will be combined into a single mosaic for each band using the MOPEX mosaicking software. Additional post-BCD processing will include distortion corrections, rotation of the individual frames, bias structure and bias drift corrections, image offset determinations via pointing refinements from the SSC pipeline, detector artifact removal, constant-level sky subtraction, and image resampling to $0.75''$ pixels using drizzling techniques. The drizzling slightly improves the final PSF over the native one.

The two largest challenges to measuring stellar emission in the extreme outer disks are the presence of foreground stars/background galaxies and the stability of the sky levels within the large maps. As explained above, we plan to minimize the first issue by constraining our sample to $|b| > 35°$. Furthermore, we have extensively explored how best to mask foreground stars and background galaxies. The optimal approach that we have converged upon relies on a two-pronged strategy. First, we identify foreground stars and background point sources using IRAF/DAOPhot. Second, we rely on SExtractor (Bertin & Arnouts 1996) to identify extended background galaxies. Empirical checks will be made via comparison with the Hα, UV, and broadband optical imaging. Next, foreground and background objects are masked using an IDL script that utilizes the SExtractor ellipses for the extended targets and the SSC-provided IRAC 2D PSFs for the foreground stars and point sources.

To assess the sky stability, we have analyzed maps from our Cycles 6 and 8 programs executed at the same imaging depth. Inspection of our mosaics, which span scales as large as $\sim 1°$, shows sky variations less than 0.001 MJy sr^{-1}. We will map the entire field of view during each AOR (two per target), and thus changes across the field due to variations in zodiacal light will be minimized. In short, we have adopted our Cycles 6 and 8 mapping strategy for this proposal, and that strategy has proven successful for a similar set of goals.

1.2.4 Data Analysis

An important parameter in deriving accurate surface brightness profiles is the sky value for each field. We will employ a curve-of-growth analysis to constrain sky levels in azimuthally averaged data. Once the sky level has been determined, azimuthal averages will allow us to probe surface brightness levels well below the single pixel detection limits (Figure 2). We will examine the surface brightness profiles at 3.6 and 4.5 μm for evidence of disk truncation, and examine the extent of the faint stellar distribution relative to the UV, optical, and Hα emission. Stellar masses will be derived from the IRAC data, and star formation histories will be calculated based on the entire multi-wavelength dataset (e.g., Panter et al. 2007).

Though NGC 5474 lacks ultra-deep NIR imaging, even a limited comparison of the outer disk ages in the XUV and non-XUV galaxies shown in Figure 2 can be illustrative. For the XUV galaxy NGC 5474, the ratio $\nu f_\nu(1528\mathring{A})/\nu f_\nu(1528\mu m)$ at $\sim 1.1 R_{25}$ indicates an

age of 8 Myr (assuming continuous star formation at solar metallicity for a double power law initial mass function, with $\alpha_{1,\mathrm{IMF}} = 1.3$ for $0.1 < m/M_\odot < 0.5$ and $\alpha_{2,\mathrm{IMF}} = 2.3$ for $0.5 < m/M_\odot < 100$; Vazquez & Leitherer 2005). Conversely, for the non-XUV system UGC 685, the same UV-to-NIR ratio at $\sim 1.2R_{25}$ implies an age of 2-3 Gyr. Obtaining deep NIR imaging for a variety of XUV and non-XUV targets will enable more detailed analyses.

The presence of 3.3 μm PAH emission in the IRAC1 band will likely be minimal due to the negligible dust present in outer disks (Gil de Paz et al. 2007b; Dong et al. 2008). Supporting this view is the low metallicity nature of outer disks ($Z/Z_\odot = 1/5 - 1/10$; Gil de Paz 2007b; Goddard et al. 2010b), coupled with the fact that low metallicity is known to depress PAH emission (e.g., Engelbracht et al. 2008; Muñoz-Mateos 2009). Indeed, no outer disk ($\sim 2R_{25}$) PAH emission is seen in a limited study of one pointing in each of five spiral galaxies, with an imaging depth similar to that proposed here (Alberts et al. 2011).

1.2.5 Management Plan

PI Dale will coordinate all efforts and serve as Technical Contact. Mosaicking and curve of growth analysis will be led by Staudaher, who has extensive experience from our Cycles 6 and 8 projects (§ 3). Gil de Paz and Thilker will provide expertise for the UV data, including post-pipeline-processed images and surface brightness profiles. Gil de Paz will also contribute deep Hα and optical broadband imaging. van Zee and Barnes will lead on comparisons to the available H$\textsc{i}$ data. Calzetti will provide expertise on using multi-wavelength data to investigate the ages and characteristics of the stellar populations of the outer disks.

1.3 Figures, Tables & References

Abadi, M.G., Navarro, J.F., & Steinmetz, M. 2006, MNRAS, 365, 747

Alberts, S. et al. 2011, 731, 28

Avila-Reese, V. & Firmani, C. 2000, RMxAA, 36, 23

Bertin, E. & Arnouts, S. 1996, A&AS, 117, 393

Brown, T.M., et al. 2008, ApJ, 685, L121

Bush, S.J., Hayward, C.C., Thilker, D., Hernquist, L., & Gurtina, B. 2010, ApJ, 713, 780

Christlein, D., Zaritsky, D., & Bland-Hawthorn, J. 2010, MNRAS, 405, 2549

Dale, D.A. et al. 2007, ApJ, 655, 863

Dale, D.A. et al. 2009, ApJ, 703, 517

Dong, H., Calzetti, D., Regan, M., Thilker, D., Bianchi, L., Meurer, G.R., & Walter, F. 2008, AJ, 136, 479

Elmegreen, B. & Hunter, D. 2006, ApJ, 636, 712

Engelbracht, C. et al. 2008, ApJ, 678, 804

Fumagalli, M. et al. 2011, ApJ, 741, 26

Gil de Paz, A. et al. 2007a, ApJS, 173, 185

Gil de Paz, A. et al. 2007b, ApJ, 662, 115

Goddard, Q.E., Kennicutt, R.C., & Ryan-Weber, E.V. 2010, MNRAS, 405, 2791

Goddard, Q.E., Bresolin, F., Kennicutt, R.C., Ryan-Weber, E.V. et al. 2011, MNRAS, 412, 1246

Gogarten, S.M., et al. 2009, ApJ, 691, 115

Governato, F. et al. 2004, ApJ, 607, 688

Herbert-Fort, S. et al. 2009, ApJ, 700, 1977

Ibata, R., Chapman, S., Ferguson, A.M.N., Lewis, G., Irwin, M., & Tanvir, N. 2005, ApJ, 634, 287

Kennicutt, R.C. 1998, ARAA, 36, 189

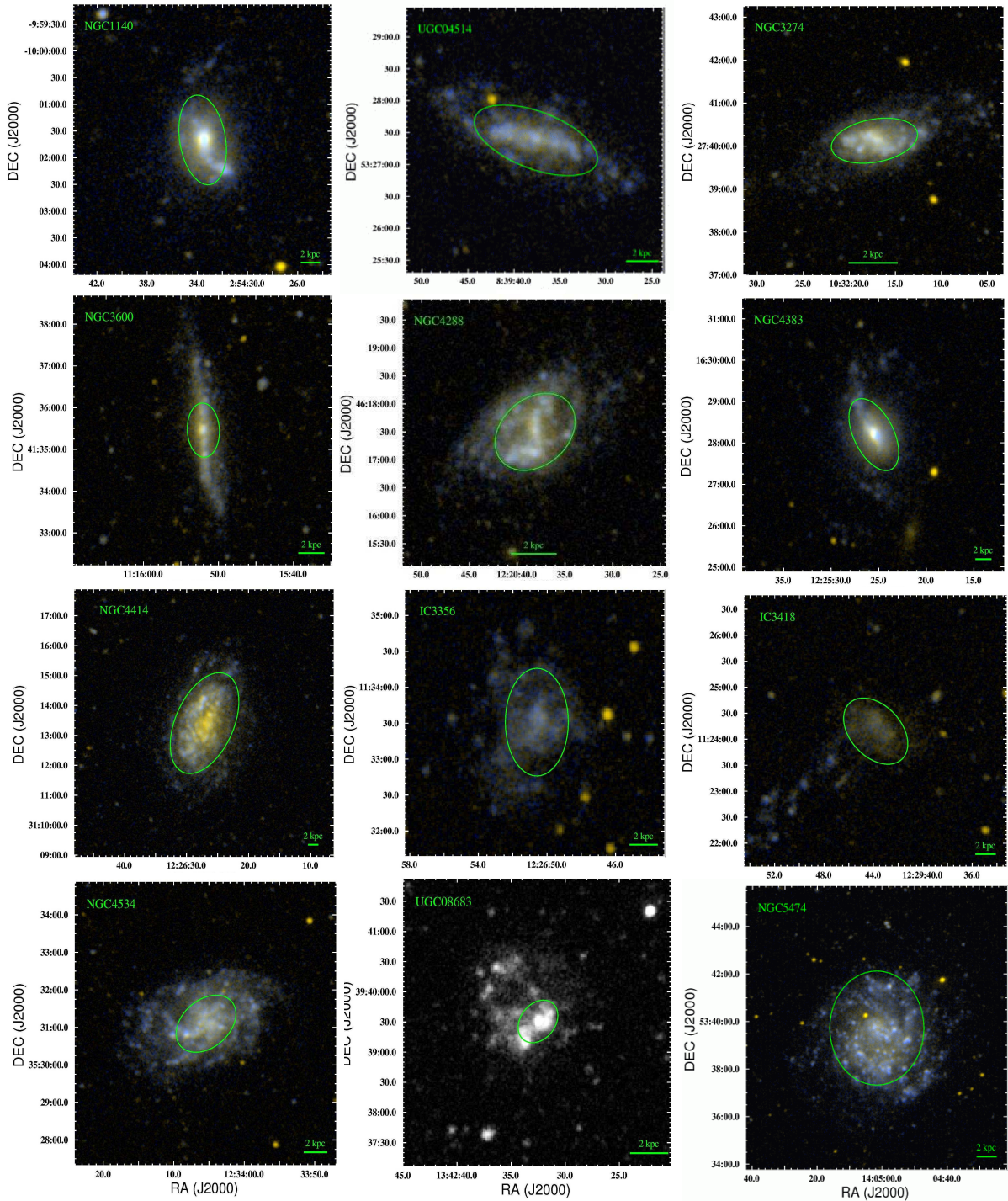Kroupa, P. & Weidner, C. 2003, ApJ, 598, 1076

Figure 1: FUV-NUV false-color images for the XUV galaxies in the sample. The UV emission extends well beyond the optical extent indicated by the $D_{25} \times d_{25}$ ellipses.

Krumholz, M.R., McKee, C.F., & Tumlinson, J. 2009, ApJ, 699, 850

Lee, J.C. et al. 2009, ApJ, 706, 599

Leroy, A.K., Walter, F., Brinks, E., Bigiel, F., de Blok, W.J.G., Madore, B. et al. 2008, AJ, 136, 2782

Martin, C.L. & Kennicutt, R.C. 2001, ApJ, 555, 301

Meurer, G.R. et al. 2009, ApJ, 695, 765

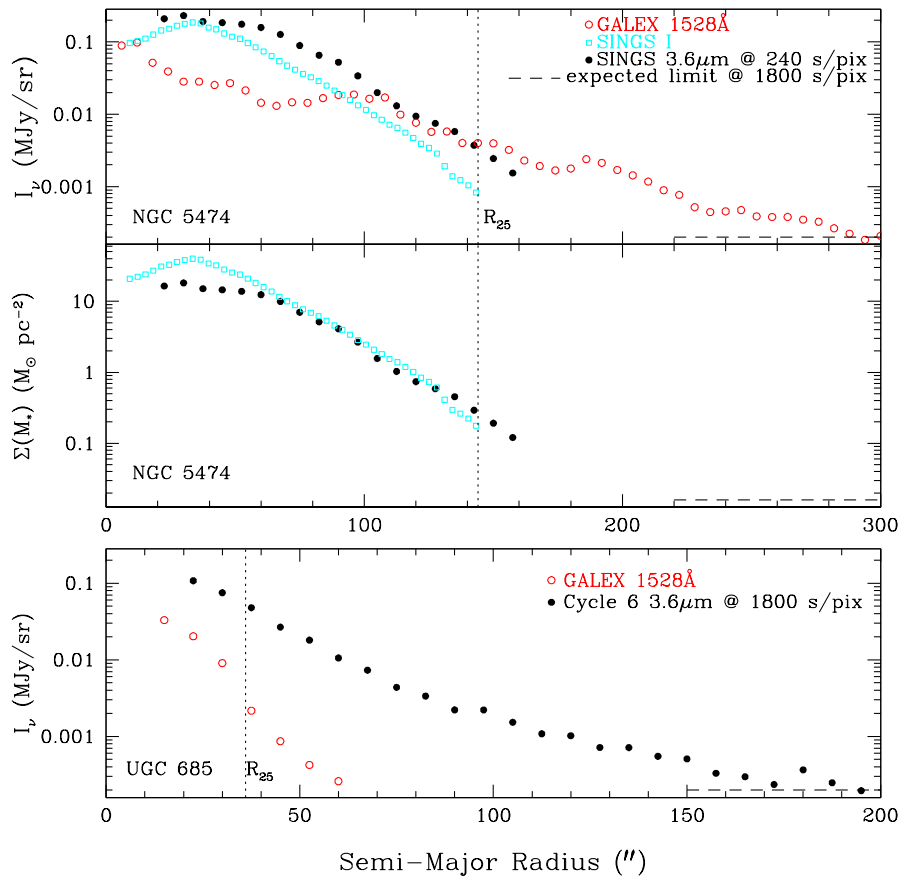Muñoz-Mateos, J.C. et al. 2009, ApJ, 701, 1965

Figure 2: **Top**: UV/optical/NIR profiles for XUV galaxy NGC 5474. The UV (open red circles) extends far beyond R_{25}. The 3.6 μm profile (filled black circles) is at the relatively shallow SINGS depth (Dale et al. 2007). The predicted surface brightness limit for our survey is indicated by the dashed line. This expectation is based on SENS-PET predictions and is consistent with the analysis of our Cycles 6 and 8 data at the same imaging depth of 1800 s/pix (see bottom panel). **Middle**: The stellar mass surface density profiles based on the 3.6 μm and I band SINGS data, assuming $M/L \sim 2-3 M_\odot/L_\odot$ for a galaxy at 10 Mpc. The expected sensitivity to stellar mass with our proposed observations goes well below that available from extant data. **Bottom**: The UV and NIR surface brightness profiles for (non-XUV) UGC 685 from our Cycle 6 program to deeply image HI-extended galaxies. These azimuthally-averaged data, taken at the same 1800 s/pix integration as that planned in this proposal, reach our targeted 3.6 μm sensitivity of ~ 0.2 kJy/sr.

Pahre, M.A., Ashby, M.L.N., Fazio, G.G., & Willner, S.P. 2005, ApJS, 154, 235

Panter, B., Jimenez, R., Heavens, A.F., & Charlot, S. 2007, MNRAS, 378, 1550

Pflamm-Altenburg, J., Weidner, C., & Kroupa, P. 2009, MNRAS, 395, 394

Pohlen, M. & Trujillo, I. 2006, 454, 759

Regan, M. et al. 2006, ApJ, 652, 1112

Robertson, B., Yoshida, N., Springel, V., & Hernquist, L. 2004, ApJ, 606, 32

Roškar, R., Debattista, V.P., Stinson, G.S., Quinn, T.R., Kaufmann, T., Wadsley, J. 2008 ApJL, 684, L79

Thilker, D.A. et al. 2005, ApJL, 619, L79

Thilker, D.A. et al. 2007, ApJS, 173, 538

Vazquez, G.A. & Leitherer, C. 2005, ApJ, 621, 695

Wang, J. et al. 2011, MNRAS, 412, 1081

Weidner, C. & Kroupa, P. 2007, MNRAS, 365, 1333

Weisz, D. et al. 2012, ApJ, 744, 44

Wright, E. et al. 2010, AJ, 140, 1882

Zaritsky, D. & Christlein, D. 2007, AJ, 134, 135

2 Brief Team Resume

Daniel A. Dale (Wyoming) is an expert on studies of star formation from low- to intermediate-redshift, as well as on the infrared spectra and panchromatic broadband spectral energy distributions of normal galaxies. He has extensive experience with *Spitzer* observations and data processing, as a CoI on SINGS, as a CoI on the Cycle 4 Local Volume Legacy Project (LVL), and as a CoI on the two Cycles 6 and 8 projects described in the next section.

Kate L. Barnes (Indiana) is in her first year of postdoctoral work. Her Ph.D. dissertation examined star formation rate indicators in the outer edges of spiral galaxies. She is PI on a Cycle 6 study of the extended disk in M 83 as well as the Cycle 8 program described in the next section.

Daniela Calzetti (UMass) is an expert on multi-wavelength observations of star formation activity in nearby galaxies. She is a member of the SINGS, LVL, among other related *Spitzer* programs.

Armando Gil de Paz (UC Madrid) is an expert on the multi-wavelength emission from normal galaxies and blue compact dwarf galaxies. He is a member of the SINGS and LVL legacy teams, and is a leading expert on GALEX observations of galaxies, including those with extended UV emission.

Shawn M. Staudaher (Wyoming) finished his second year of graduate school; his thesis would focus on this project. He spent the previous two years as a post-baccalaureate research assistant with Dale. He has led the IRAC data processing and mosaic construction for the Cycle 8 and two Cycle 6 programs described in the following section.

David Thilker (Johns Hopkins) is an expert on the multi-wavelength properties of nearby galaxies. His discovery of extended UV emission in M 83 has led to intense efforts to understand star formation in galaxy peripheries.

Liese van Zee (Indiana) is an expert on galaxy formation and evolution with an emphasis on investigating the links between star formation, elemental enrichment, and gas distribution and kinematics in star-forming galaxies. She has extensive experience working with multi-wavelength data sets (UV, optical, IR, and radio). She is PI of a program in both Cycle 6 and Cycle 8, as described in the following section, and is CoI on LVL.

Selected Related Publications

The Calibration of Far-Infrared Monochromatic Star Formation Rate Indicators
    Calzetti et al. 2010, ApJ, 714, 1256
Herschel Far-infrared and Submillimeter Photometry for the KINGFISH Sample of nearby Galaxies
    Dale et al. 2012, ApJ, 745, 95
The *Spitzer* Local Volume Legacy: Survey Description and Infrared Photometry
    Dale et al. 2009, ApJ, 703, 517
The GALEX Ultraviolet Atlas of Nearby Galaxies
    Gil de Paz et al. 2007, ApJS, 173, 185
A Search for Extended Ultraviolet Disk (XUV-Disk) Galaxies in the Local Universe
    Thilker et al. 2007, ApJS, 173, 538
Spectroscopy of Outlying Hɪɪ Regions in Spiral Galaxies: Abundances and Radial Gradients
    van Zee et al. 1998, AJ, 116, 2805

3   Summary of Existing Programs

Kate Barnes is the PI of 60116, a 30.2-hour Cycle 6 Warm Mission program to probe the extended older stellar population in M 83. The data have been post-pipeline processed, and we have optimized the creation of their image mosaics, developed routines for masking foreground stars and background galaxies, extracted surface brightness profiles, and compared the radial extent of the older population to the H I radius. The results appeared in her recently completed dissertation, and a manuscript is in preparation.

Daniela Calzetti is the PI of 20289 and 30753, Cycles 2 and 3 programs to probe the star formation and dust content in the outer parts of nearby galaxies. Results have been published (Dong et al. 2008) and (Alberts et al. 2011).

Liese van Zee is the PI of 60094, a 69.7-hour Cycle 6 Warm Mission program to probe the older stellar population in the outskirts of galaxies with extended H I disks. The observations for this program were completed in August 2010. The data have been post-pipeline processed, and we have optimized the creation of their image mosaics, developed routines for masking foreground stars and background galaxies, extracted surface brightness profiles, and compared the radial extent of the older population to the H I radius. Results are included in this proposal. van Zee is also PI of 80025, a 1005.3-hour Cycle 8 program to map the extended disks in a sample of normal galaxies. 71% of the AORs have been observed and an additional 20% are in the scheduling queue. Data processing is underway, and preliminary analysis has begun on optimal foreground star subtraction and faint outer disk detection.

Daniel Dale is Technical Contact for the above programs led by Barnes and van Zee. Dale is leading the data processing efforts on these programs.

4   Observation Summary Table

Galaxy	Position (J2000)	$D_{25} \times d_{25}$ (arcmin)	D_{UV}/D_{25}	# grid points	AOR (hrs)	$f(K_\mathrm{s})$ (Jy)	Type
NGC1140	025433.6−100140	1.7×0.9	3.0	8x 8	4.1	0.042	XUV 2
UGC04514	083937.7+532723	2.1×0.9	2.2	8x 8	4.1		XUV 1
NGC3274	103217.3+274008	2.1×1.0	3.0	8x 8	4.1	0.036	XUV 2
NGC3600	111552.0+413527	1.3×0.8	3.6	8x 8	4.1	0.055	XUV 1
NGC4288	122038.1+461730	1.6×1.2	2.8	8x 8	4.1	0.032	XUV 1
NGC4383	122525.5+162812	1.9×1.0	3.5	8x 8	4.1	0.106	XUV 1
NGC4414	122627.1+311325	3.6×2.0	1.9	13x13	10.6	1.110	XUV 1
IC3356	122650.5+113332	1.5×0.9	2.4	8x 8	4.1		XUV 1
IC3418	122943.8+112409	1.5×1.0	2.7	8x 8	4.1		XUV 1
NGC4534	123405.4+353106	1.9×1.3	3.2	8x 8	4.1	0.150	XUV 2
UGC08683	134232.5+393930	0.8×0.6	5.3	8x 8	4.1		XUV 1.5
NGC5474	140312.5+542056	4.8×4.3	2.2	16x16	16.0	0.114	XUV 1.5

There are 67.3 hrs total requested for this observing program. We are submitting final AORs for this program.

5   Modification of the Proprietary Period

No modification to the proprietary period is requested for this program.

6   Summary of Duplicate Observations

There are no duplicate observations. Observations by the SINGS (P00159), LVL (P40204), and S^{4}G (P61060-8) programs for UGC 04514, NGC 3274, NGC 3600, NGC4288, IC 3356, NGC 4534, and NGC 5474 do not have the depth (2×4×30 s/pix=240 s/pix) and field of view to constitute our observations as duplications. A few programs have observed a handful of other galaxies, and again our duplications are deeper and more extended to not be considered duplications: NGC 1140 (P00059), NGC 4383 (P30945), NGC 4414 (P00069), IC 3418 (P03418).

7   Summary of Scheduling Constraints/ToOs

There are no scheduling constraints or ToOs in this program.